Aging and hygroscopicity variation of black carbon particles in Beijing measured by a quasi-atmospheric aerosol evolution study (QUALITY) chamber

Jianfei Peng[1, 2]*, Min Hu[1, 3]*, Song Guo[1,2], Zhuofei Du[1], Dongjie Shang[1], Jing Zheng[1], Jun Zheng[2], Limin Zeng[1], Min Shao[1], Yusheng Wu[1], Don Collins[2], Renyi Zhang[1,2]*

[1]State Key Joint Laboratory of Environmental Simulation and Pollution Control, College of Environmental Sciences and Engineering, Peking University, Beijing, China 100871

[2]Department of Atmospheric Sciences, Texas A&M University, College Station, Texas, USA 77843

[3]Beijing Innovation Center for Engineering Sciences and Advanced Technology, Peking University, Beijing, China 100871

*To whom correspondence should be addressed. E-mail: pengjianfeipku@gmail.com (Jianfei Peng); minhu@pku.edu.cn (Min Hu); renyi-zhang@geos.tamu.edu (Renyi Zhang)

Abstract. Measurements of aging and hygroscopicity variation of black carbon (BC) particles in Beijing were conducted using a 1.2 m^3 quasi-atmospheric aerosol evolution study (QUALITY) chamber, which consisted of a bottom flow chamber where ambient air was pulled through continuously and an upper reaction chamber where aging of BC particles occurred. Within the reaction chamber, transmission of the solar ultraviolet irradiation was approximately 50% - 60%, wall loss of primary gaseous pollutants was negligible compared with the replenish rate by gas exchange, and BC exhibited a half-lifetime about 3-7 hours. Typically, equilibrium for the primary gases, temperature, and relative humidity between the reaction chamber and ambient air was established within 1 hour. Rapid growth of BC particles was observed, with an average total growth of 77±33nm and average growth rate of 26±11 nm h^{-1}. Secondary organic aerosols (SOA) accounted for more than 90% of the coating mass. The O/C ratio of SOA was 0.5, lower than the ambient level. The hygroscopic growth factor of BC particles decreased slightly with an initial thin coating layer because of BC reconstruction, but subsequently increased to 1.06-1.08 upon further aging. The κ (kappa) values for BC particles and coating materials were calculated as 0.035 and 0.040 at the subsaturation and supersaturation conditions, respectively, indicating low hygroscopicity of coated SOA on BC particles. Hence, our results indicate that initial photochemical aging of BC particles does not appreciably alter the particle hygroscopicity in Beijing.

1 Introduction

Atmospheric aerosols undergo continuous and complicated transformation during their residence time in the atmosphere. The aging of aerosols is likely resulted from both physical (i.e., coagulation, condensation, equilibrium partitioning, and evaporation) and chemical (i.e., photochemical gas-phase oxidation and multi-phase reactions) processes (Zhao et al., 2006; Qiu et al., 2013; Zhang et al., 2015). Also, there are typically large variations in the particle properties (i.e., size, mass, chemical composition, morphology, and optical and hygroscopic parameters) during aging, significantly influencing the aerosol impacts on visibility, human health, weather, and climate (Jacobson, 2001; Guo et al., 2014). A better understanding of the aging process of aerosols in the atmosphere is critical in atmospheric and climate research.

For example, the scientific interest in the climate effects of black carbon (BC) has remained, since BC is the strongest absorber of visible solar radiation (Wang et al., 2013). BC solar absorption represents a central issue in climate change research, since the synthesis of satellite, in situ, and ground observations shows that the global solar absorption (direct radiative forcing or DRF) by BC is as much as 0.9 $W\cdot m^{-2}$, second only to that of CO_2 (Jacobson, 2001; Bond et al., 2013; IPCC, 2013). BC also represents an important component of air pollution for large parts of the world (Zhang et al., 2015). The properties of BC are considerably modified during aging, including the size, mass, morphology, and optical and hygroscopic parameters (Khalizov et al., 2009; Xue et al., 2009a). Enhanced light absorption of BC particles during aging not only contributes to atmospheric stabilization and exacerbation of haze formation, but also imposes large positive radiative forcing on climate (Peng et al., 2016). Furthermore, the variation in hygroscopicity during aging also regulates the lifetimes of BC particles. Hygroscopic particles serve efficiently as cloud condensed nuclei (CCN), affecting the formation, longevity and albedo of clouds (Yuan et al., 2008; Wang et al., 2011). Also, deposition of BC particles, via in-cloud scavenging and wet deposition, depends highly on the particle hygroscopicity (Bond et al., 2013). In addition, the hygroscopicity also affects the aqueous-phase reactions of atmospheric pollutants (Ervens et al., 2011; Wang et al., 2016). Previous studies using hygroscopic tandem differential mobility analyzer (H-TDMA) instruments have shown that coating of hydrophilic materials significantly increases the hygroscopic growth factor of BC particles (Saathoff et al., 2003; Khalizov et al., 2009; Guo et al., 2016). The ability of BC particles to form CCN also enhanced after coating of hydrophilic materials (Kuwata et al., 2007; Tritscher et al., 2011; Ma et al., 2013; Wittbom et al., 2014). The activation supersaturation depends on the particle size, hygroscopicity of coating materials, and the coating thickness (Ma et al., 2013). The coating materials in the previous experiments include sulfuric acid (Zhang and Zhang, 2005; Khalizov et al., 2009), oxidation products from biogenic and anthropogenic hydrocarbon species (Saathoff et al., 2003; Ma et al., 2013; Khalizov et al., 2013), or secondary organic aerosols (SOA) from single emission source (Tritscher et al., 2011). However, there still exist uncertainties for parametrization of the BC lifetime in atmospheric models, because of insufficient constraints on the hydrophobic to hydrophilic conversion of BC particles under variable ambient conditions.

Atmospheric field measurements have been performed to evaluate aging of particles on different platforms, e.g., ground, aircraft, and cruise (Moffet and Prather, 2009; DeCarlo et al., 2010; Peng et al., 2014; Liu et al., 2015) and over different spatial scales (intensive campaigns or long-term measurements). Typically, a wide variety of state-of art instruments are employed to characterize the changes of the chemical and physical properties of aerosols. On the other hand, field measurements at fixed sites are affected by transport, local emissions, and chemistry, and quantification of the particle parameters during aging involves complex decoupling of the various processes (Peng et al., 2016). In particular, it is challenging to isolate the chemical processes from those related to meteorology (i.e., transport and mixing) and emissions.

The methods of environmental chambers or reactors have been widely employed in atmospheric chemistry research, including photochemical oxidation of volatile organic compounds (VOCs) (Zhang et al., 2000), formation and growth of aerosols (Claeys, 2004; Kalberer, 2004), nucleation of nanoparticles (Zhang et al., 2004; Wang et al., 2010; Zhang et al., 2012), aging of BC particles (Zhang et al., 2008), and cloud formation (Ruehl et al., 2016). Dependent of the scientific objectives, the designs of environmental chambers and reactors vary considerably (Zhang et al., 2015). However, few of the previous experimental methods have characterized the evolution of aerosols under the ambient conditions.

In this study, we present measurements of aging and hygroscopicity variation of BC particles in Beijing using a quasi-atmospheric aerosol evolution study (QUALITY) chamber (Reed, 2010; Peng et al., 2016). The performance of the QUALITY chamber for mimicking the ambient gaseous concentrations (i.e., the wall loss, and gas mixing rate), ultraviolet transmission, and meteorology parameters (i.e., temperature and relative humidity, RH) has been evaluated.

2 Experimental method

The 1.2 m^3 QUALITY chamber was employed to study BC aging under ambient conditions (Fig. 1). The two-layer chamber was comprised of an inner layer of 0.13 mm Perfluoroalkoxy alkane (PFA) Teflon and an outer rigid 5.6 mm thick acrylic shell (Cyro Industries Acrylite, OP-4). Both Acrylite OP-4 Acrylic and PFA Teflon allowed for efficient ultraviolet (UV) transmission in UV-B (280-315 nm) and UV-A (315-400 nm) ranges. When exposed to sunlight, the UV light transmitted through the chamber wall and initiated photochemical reactions inside the chamber.

The two individual subdivisions of the QUALITY chamber included a bottom flow chamber, where ambient air was pulled through continuously over each experiment, and an upper reaction chamber, where aging of BC particles occurred (Fig. 1). The two chambers were separated by a 5 μm thick semi-permeable expanded polytetrafluoroethylene (e-PTFE) membrane with high degrees of chemical resistivity, microporosity, nonpolarity, and thermal stability. Gaseous species penetrated the membrane by either bulk gas flow or diffusion. The permeability of the e-PTFE was greater than 90 % for nearly all the tested volatile organic components (Fig. S1) and other gaseous pollutants, i.e., SO_2, NO_x, O_3 and CO. Particles, on the other hand, were blocked from penetration into the reaction chamber. The filtration efficiency of the e-PTFE membrane was measured to be over 99.5% for particles larger than 15 nm. During each chamber experiment, ambient air was pulled through the flow chamber continuously and gases in lower chamber permeated through the membrane into the reaction chamber. Hence, an environment that continuously captured the ambient gas concentrations without the presence of ambient particles was created inside the reaction chamber. Since the chamber was continuously exposed to ambient gas concentrations during experiments, gases lost due to reaction, deposition or adsorption to the seed aerosols within the reaction chamber were steadily replenished by the exchange with the flow chamber. Several sampling ports were set at the side of the reaction chamber for injection of seed particles or sampling during experiment.

Seed particles were introduced in the reaction chamber via an injection line (Fig. S2). To investigate the growth of BC particles under ambient condition, monodisperse BC particles were injected into the QUALITY chamber. BC particles were generated by incomplete combustion of propane fuel in a custom-made laminar diffusion burner (Santoro et al., 1983; Qiu et al., 2012). The aerosol stream sequentially passed through a 300°C heater to evaporate the semi-volatile organic compounds in the particle phase, a Nafion dryer to remove excess moisture in the flow, and four one-meter-long cylinders containing both alumina spherules coated with potassium hypermanganate and activated carbon to remove all the gaseous pollutants (i.e., VOCs, H_2S, SO_2, NO_x, O_3). The combined measurement of particle size distribution, density and chemical composition exhibited that organics accounted for less than 10% of fresh BC mass concentration. Moreover, the single scattering albedo (SSA) of fresh BC particles was only 0.1, further confirming that few organic coatings exited on fresh BC particles after treatment. The measured removal efficiency in the cylinders for SO_2, NO and NO_2 were 99.2%, 100%, and 99.9%, respectively. The aerosol stream was then introduced through an ionizer and into a differential mobility analyzer (DMA, model 3081, TSI, Inc.) with stable voltage to create a monodisperse BC particles flow. A suite of high time resolution state-of-the-art aerosol instruments simultaneously measured a comprehensive set of BC properties throughout the BC aging process (Table S1). The particle diameter, mass, chemical composition, hygroscopicity and ability as cloud condensation nuclei (CCN) were measurement by a scanning mobility particle sizer (SMPS), a differential mobility analyzer–aerosol particle mass analyzer (DMA-APM) system, a high-resolution time-of-flight aerosol mass spectrometer (HR-ToF-AMS), a humidified tandem differential mobility analyzer (HTDMA) system, and a could condensation nuclei counter (CCNC), respectively. Detail information of the instruments is provided in the supplementary material and previous publications (DeCarlo et al., 2006; Khalizov et al., 2009). Specific measurement procedures in this study are discussed below.

DMA-APM measurement. The DMA-APM was used to measure the effective density of BC particles (Pagels et al., 2009). Before any DMA-APM measurement, a SMPS scan was made to obtain the size distribution of particles inside the chamber. The particle size distribution was then fitted with a lognormal Gaussian distribution to derive the peak diameter. During a DMA-APM measurement, the aerosol flow passed through DMA with a fixed voltage to select particles with a fixed diameter. The APM then measured the mass distribution of the selected particles with the same diameter, and the effective density of these particles was obtained by fitting the mass distribution with a normal Gaussian distribution.

DMA-CCN measurement. Similar to the density measurements, CCN activation was also measured on the basis of monodisperse particles with a peak diameter. A DMA with a fixed voltage selected particles with a peak diameter. Both a CPC and a CCN counter were placed in parallel after the DMA to simultaneously measure the total particle number concentration (N_{cn}) as well as the activated number concentration (N_{ccn}) at a fixed supersaturation. The activation fraction of the BC particles with peak diameter is calculated as:

$$f_{CCN} = \frac{N_{CN}}{N_{CCN}} \qquad (1)$$

Several gradients of supersaturation were set for the CCN counter, with each one being 6 min. This method yielded a steeper curve of the CCN activation rate, which was employed to estimate the particle diameter with 50% activation fraction (D_{50}) and the kappa value.

Prior to each experiment, the QUALITY chamber was flushed by zero air for more than 40 hours to ensure a clean condition and covered with two layers of anti-UV cloth to shield it from sunlight. In the beginning of each experiment, monodisperse BC particles were introduced into the chamber. The injection of BC particles typically lasted for 1 to 2 hours. During the injection period, zero air passed through the bottom chamber continually to remove any possible remaining gaseous pollutant that were removed by the activated carbon. After the injection, ambient air was pulled through the bottom chamber at a flow rate of about 50 L min^{-1} for at least half an hour in order to produce a quasi-ambient condition inside the chamber. Finally, the anti-UV cloth was removed, and BC particles underwent aging inside the reaction chamber. A charged zero air stream continuously passed through the space between the two chamber layers to reduce particle wall loss. Various properties of BC particles, including the particle diameter, mass, chemical composition, hygroscopicity, and optical coefficients, were simultaneously measured by a suite of state-of-art aerosol instruments in every 0.5 - 1 hour. Ambient particles and chamber particles were measured alternately every 30 min. The aging experiments lasted for about 2-6 hours depending on the initial BC concentrations and ambient conditions.

The BC aging experiments were conducted from August 18th to October 17th, 2013 at an urban site (PKUERS) located on the campus of Peking University in the northwestern Beijing (39.99°N, 116.31°E) (Hu et al., 2012).

3. Characterization and Validation of the QUALITY chamber

3.1 Wall loss of gases and aerosols

To evaluate the wall loss of both particles and gases in the QUALITY chamber, different gaseous pollutants and particles were introduced into the chamber separately and the decay of their concentration inside the chamber was measured by gas analyzers and SMPS, respectively. All of the ports connected to the ambient air were closed to ensure an enclosed system in the reaction chamber.

Particles with different chemical composition exhibited different wall loss rates. Monodispersed BC particles with different diameters showed a small half-lifetime (τ) of about 4-7 hours (Reed, 2010). Aerosol nucleation also occurred inside the chamber likely from organic species (Zhao et al., 2009), which corresponded to a half time of about 3.5 hours (Fig. S3), because the nucleated particles inside the chamber was neutral with a slow electrostatic loss to the wall.

Gas species had a longer residence time inside the chamber. Toluene and isoprene did not show obvious wall loss during a two-day experiment (Reed, 2010). O_3, SO_2 and NO_x decreased by 50% inside the chamber after more than 20 hours, suggesting slow loss. Since the loss rate of these primary gaseous pollutants was much slower than the gas exchange rate between the chamber, the loss of gases was replenished by the exchange with the flow chamber.

3.2 UV transmission

The QUALITY chamber contained two layers of walls, an acrylic shell layer and a PFA Teflon layer. Since the QUALITY chamber used sunlight as the photochemical origin, the transmission spectra of the two-layer walls was of great important for the photochemical reactions inside the reaction chamber.

The transmission efficiencies of each material were measured using an ultraviolet-visible (UV-Vis) spectrophotometry (PerkinElmer Inc., model 552). As shown in Figure 2, the Teflon film exhibited stable transmission efficiency of about 60% in the focused wavelength range. The Acrylic shell, however, showed very low transmission efficiency when the wavelength range was shorter than 270 nm, and high transmission efficiency (nearly 90%) when the wavelength range was longer than 300 nm. In general, approximately 60% of the UVA irradiation (315-400 nm range) and 50% of the UVB irradiation (280-315 nm range) penetrated through the chamber walls, allowing photochemical processes to take place in the upper reaction chamber.

A NO_2-photolysis experiment was also conducted to characterize the UV transmission of QUALITY chamber. NO_2 was introduced inside the chamber at a clean and sunny day. Reactions among NO_2, NO and O_3 will occur as the following equations:

$$NO + O_3 \rightarrow NO_2 + O_2 \qquad (2)$$

$$NO_2 \overset{hv}{\rightarrow} NO + O \qquad (3)$$

$$O + O_2 \rightarrow O_3 \qquad (4)$$

By simultaneously monitoring the concentrations of NO_2, NO and O_3 inside the chamber, the photolysis constant of NO_2, $J(NO_2)$, inside the chamber was estimated. The photolysis constant of NO_2 inside the chamber was on average 55% of that in the ambient air, in agreement with the transmission spectra measurement, further confirming that the two-layer chamber walls allowed 50% - 60% of solar irradiation in the UV range into the reaction chamber.

3.3 Gas concentrations in the reaction chamber

To investigate the VOCs concentration inside the reaction chamber after the injection of BC particles, both the chamber and ambient air were sampled with VOC canisters just before the BC aging experiment started. These canisters were then analyzed by a gas chromatography-mass spectrometer / flame ionization detector (GC-MS/FID, HP inc.) system

(Liu et al., 2008). The concentrations of VOCs containing 4 or more carbons are illustrated in Figure 3. Slightly higher concentrations of several VOCs in the QUALITY chamber, e.g., n-butane, n-pentane, toluene, were observed compared with those in the ambient air, duo to the co-injection of a small amount of VOCs together with BC particles into the chamber. Nevertheless, the average increase of the VOC concentrations was only 16% or 0.1 ppb for all focused VOCs species, with the largest increase of 35% or 0.36 ppb, suggesting the insignificant influence of soot burner on VOCs concentrations and SOA formation in the chamber.

Additional experiments were conducted to characterize the exchange time scale for gases in the QUALITY chamber. The chamber was firstly cleaned and flushed with zero air for 40 hours. Ambient air was then pulled through the bottom chamber (Fig. 4), and the concentrations of gaseous pollutants, including O_3, NO_x, CO, and SO_2, were measured alternatively in the ambient air and in the upper chamber. In the beginning of the experiment the concentrations of all gaseous species were lower than those in the ambient air. After ambient air was pulled through the bottom chamber (labeled as the black dots in Fig. 4), the concentrations of the gaseous pollutants in the reaction chamber increased sharply. For example, the CO concentration inside the chamber was approximate 70% of that the ambient concentration after 30-min mixing. The concentrations inside the chamber and ambient air exhibited little difference after 1-hour mixing (Fig. 4c). Hence, the QUALITY chamber well replicated the ambient gas concentrations. The gas exchange rate between the bottom and reaction chambers was calculated to be approximately 0.06 min^{-1}.

3.4 Temperature and RH

The greenhouse effect for an outdoor chamber typically increases the temperature and decreases the RH inside the chamber. For the QUALITY chamber, however, heat produced by the greenhouse effect inside the chamber was effectively taken away as the ambient air continuously passed through the bottom chamber and exchanged with air in the upper chamber. As illustrated in Figure 5, there was little difference in temperature or RH inside and outside the chamber, when the chamber experiments lasted for more than 1 hour, suggesting that the QUALITY chamber effectively captured the ambient temperature and RH.

3.5 Sulfuric acid production

Though gaseous pollutants such as SO_2, O_3, NO_x and VOCs penetrated into the reaction chamber from the bottom chamber through the semi-permeable membrane, low volatile and sticky gases, i.e., sulfuric acid, were unlikely to penetrate through the membrane (Fortner et al., 2004). To characterize sulfuric acid production inside the chamber, we conducted a special experiment by pulling ambient air into the bottom chamber, while injecting SO_2 directly into the reaction chamber. The experiment was conducted around noon on a clean day when the O_3 concentration was around 50 ppb. A custom-made atmospheric pressure-ion drift chemical ionization mass spectrometry (AP-ID-CIMS) (Fortner et al., 2004; Zheng et al., 2010) was used to directly measure the concentration of gaseous sulfuric acid. Fig. 6 shows a good correlation between SO_2 and gaseous H_2SO_4 inside the chamber, suggesting that the QUALITY chamber well simulated the formation of low volatile gaseous species and hence the photochemical processes.

4. BC evolution in the QUALITY chamber

Time series of the ambient PM, gas, and meteorology parameters of ambient air during chamber experiment period are illustrated in Figure 7. Except for the last experiment conducted on October 17th, all experiments were conducted between August 18th, 2013 and September 21st, 2013. During this period in Beijing, strong photochemical reactions and frequent heavy pollution events occurred (Huang et al., 2010; Zhao et al., 2013). Temperature and RH during this period (August 18th to September 21st) varied from 24°C to 38°C and from 20 % to 90 %, respectively. The average concentration of $PM_{2.5}$, SO_2 and NO_x were 60 ± 45 μg m^{-3}, 3.2 ± 2.6 ppb and 33.9 ± 20.9 ppb, respectively.

The red shaded areas in Figure 7 represent the period of the nine chamber experiments. In general, chamber experiments were conducted in the afternoon of relatively clean and sunny days, when strong solar radiation led to fast photochemical reactions. There were two experiments conducted under polluted days, e.g., the experiments on October 22rd and September 11th. Table 1 summaries the conditions of the experiments. Totally, 10 BC aging experiments were conducted, including four experiments using BC particles with initial mobility diameter of 100 nm, three experiments using 150 nm particles, and three using 220 nm BC particles. The average concentrations of $PM_{2.5}$ and NO_x over each chamber experiment were only 9 to 69 μg m^{-3} and 9 to 41 ppb, respectively. The concentrations of VOCs, such as toluene and m/p-xylene were relatively low during most of the experiments compared with severe pollution episodes in Beijing (Guo et al., 2014). $J(O^1D)$ and O_3 exhibited higher values during the chamber experiments. The average $J(O^1D)$ values and O_3 concentrations ranged from 3.2×10^{-6} s^{-1} to 21.1×10^{-6} s^{-1} and 26 to 92 ppb, respectively.

4.1 BC growth

To quantify the growth of BC particles, several parameters were used to describe the properties of BC particle, including the effective density, mobility diameter and mass equivalent diameter. Material density (ρ_m) is the average density of the solid and liquid material in the particle. Assuming that the volume of the species coexisting in an individual particle does not change upon mixing, the density of an internally mixed particle is calculated using the material densities and mass concentrations of particulate constituents (DeCarlo et al., 2004; Pagels et al., 2009),

$$\rho_m = \frac{\sum_{species} m_i}{\sum_{species} V_i} = \frac{\sum_{species} m_i}{\sum_{species} \frac{m_i}{\rho_i}} = \frac{\sum_{species} MC_i}{\sum_{species} \frac{MC_i}{\rho_i}} \qquad (5)$$

where ρ_i is the material density of species i, V_i is its volume, m_i is its mass, and MC_i is its mass concentration. This approach is based on the assumption that there is no void space enclosed within the particle envelope. Hence, the material density is larger than the true particle density with internal voids in particles. In this study, ρ_m is calculated from the chemical composition of coating materials measured by AMS. A value of 1.35 for the material density of SOA formed during chamber experiment was obtained by directly measuring the density of newly form particles inside the chamber via DMA-APM system.

Effective density (ρ_{eff}) is defined as the ratio of the measured particle mass (m_p) to the particle volume calculated assuming a spherical particle with a diameter equal to the measured mobility diameter (D_m) (DeCarlo et al., 2004; Pagels et al., 2009; Xue et al., 2009b):

$$\rho_{eff} = \frac{6m_p}{\pi D_m^3} \tag{6}$$

In this study, m_p of BC particles was measured by the APM and mobility diameter (D_m) was measured by the DMA. The effective density reflects the information on both particle density and shape. If particles are spherical in the absence of internal void, the effective density equals the material density. If particles are non-spherical, the calculated volume and volume concentration are larger than the true values, and the effective density is less than true particle and the material density.

Figure 8 exhibits the change of particle density and diameter in three typical BC aging experiments using BC particles with the initial diameter of 100 nm, 150 nm, and 220 nm (experiment #4, #5, and # 9 in Table 1, respectively). The average $PM_{2.5}$ concentrations in these experiments were 40, 27, and 12 μg m^{-3}, respectively, suggesting relatively clean conditions during the experiments. In all three experiments, aging of BC particles occurred between 13:00-14:00 and 17:00 in the afternoon. The highest $J(O^1D)$ value varied from 1.7 to 2.4×10^{-5} s^{-1} and decreased generally over the experiment period. Average O_3 concentrations during the three experiments were 68, 83 and 54 ppb, respectively, indicating strong oxidation during the experiment periods.

For three initial D_m of 100 nm, 150 nm, and 200 nm, the ranges of effective density of fresh BC particles in each experiment were 0.43-0.50 g cm^{-3}, 0.34-0.34 g cm^{-3}, and 0.24-0.32 g cm^{-3}, respectively, indicating highly fractal BC aggregates (Zhang et al., 2008). The small variation for particles with the same D_m also demonstrates the consistency of fresh BC morphology in different experiments. After aging of 1 hour, ρ_{eff} of BC particles in the three experiments increased to approximately 1.2 g cm^{-3}, suggesting that formation of the secondary components changed the morphology from chain-like BC particles into a more compact shape (Zhang et al., 2008; Peng et al., 2016). The morphology change was further confirmed by a decrease of D_m, particularly for larger BC particles that were more fractal than smaller BC particles.

As the D_m is largely influenced by the particle morphology, we utilized the parameter of mass equivalent diameter (D_{me}) to describe the growth of particles. Based on the mobility diameter (D_m), material density (ρ_m) and effective density (ρ_{eff}), the D_{me} is calculated assuming that particles are compact and with a spherical morphology (DeCarlo et al., 2004):

$$D_{me} = \sqrt[3]{\frac{\rho_{eff}}{\rho_m}} D_m \tag{7}$$

The change in the mass equivalent diameter (ΔD_{me}) during BC aging is defined as the total coating thickness, and the ratio of the total coating thickness to the initial mass equivalent diameter ($\Delta D_{me}/D_{me,0}$) is defined as the coating fraction.

The initial D_{me} of fresh BC particles with initial D_m of 100, 150 and 220 nm were 61, 84 and 114 nm, respectively. In contrast to the mobility diameter, D_{me} increased continuously during the entire experiment. After 3-4 hours, D_{me} in the three experiments increased to 133, 169 and 197 nm, respectively (Fig. 8), with the average growth rates of 19, 29 and 31 nm h^{-1}. Higher growth rates in D_{me} occurred around noontime, when the $J(O^1D)$ value was higher and the photochemical reaction was stronger. On the other hand, much less growth rate was observed during late afternoon or with cloud coverage (As shown in Fig. 8c at 15:00), indicating that the growth was driven by photochemical reactions.

The increases of the particle density and diameter in all the experiments are summarized in Table 2. Fast aging of BC particles occurred in all experiments. The total growth of D_{me} ranged from 40 nm to 152 nm within 3-6 hours, with an average growth of 73 nm. The average growth rate was 26±11 nm h^{-1}, demonstrating large secondary production under the ambient conditions in Beijing. The largest growth rate (ΔD_{me} = 152 nm) was observed in experiment #8, when solar irradiation was the strongest among all experiments (Table 2).

Correlation analysis was made between the average growth rate of BC particles ($\Delta D_{me}/\Delta t$) with O_3, $PM_{2.5}$, $J(O^1D)$, and temperature during the different experiments (Fig. S4). The growth rate of BC particles exhibits no correlation with O_3 concentration (R^2=0.00), weak negative correlation with $PM_{2.5}$ concentration (R^2 = 0.25), and strong positive correlations with $J(O^1D)$ (R^2 = 0.80) and temperature (R^2 = 0.67), indicating the importance of photochemical production on the BC coating materials.

4.2 Chemical composition of coating materials

Particle composition measurements by AMS during chamber experiments reveal a majority of coating materials (above 90%) as SOA (Fig. 8). The concentration of SOA inside the chamber reached up to 9 μg m^{-3} in several experiments, suggesting fast formation of SOA via gas phase oxidation of VOCs. The SOA formation in Beijing is likely attributed to a large amount of anthropogenic aromatic VOCs (Peng et al., 2017).

The elemental compositions of OA inside the chamber, i.e., the oxygen to carbon (O/C) ratio and the hydrogen to carbon (H/C) ratio, were calculated based on the updated ambient calibrations (He et al., 2011; Canagaratna et al., 2015). The H/C and O/C ratios of organics for coating on BC particles exhibit notable trends during the aging process. Figure 9A shows an example of the evolution of H/C and O/C ratios in experiment #8. The data were corrected for the CO_2 concentration in the chamber, which were introduced into the chamber with BC particles and influenced the abundance of m/z = 28 and 44 in the AMS mass spectra. The H/C ratio decreased from 1.73 to 1.45 over six hours. Accordingly, the O/C ratio increased from 0.32 to 0.50 during the same time, revealing that further oxidation of SOA occurred in the latter part of the experiment. The lower final O/C ratio in the chamber experiment (0.5) than that under the ambient conditions (Hu et al., 2016) implies that there is oxidation on a longer timescale or by the aqueous pathway for the formation of highly oxidized SOA in the ambient air (Zhang et al., 2015).

Furthermore, the mass spectra of OA inside the chamber shows strong correlation with the less-oxidized oxygenated organic aerosols (LO-OOA) derived from field measurements in Beijing (Hu et al., 2016), which likely arose from oxidation of aromatic VOCs emitted from vehicles (Peng et a., 2017). The correlation coefficient (R^2) initially was 0.88 and raised to 0.99 sharply (Fig. 9B), indicating that the chamber well simulated the formation of LO-OOA.

In our study, the secondary inorganic aerosols, i.e., sulfate, nitrate and ammonium, only accounted for less than 10% of the coating materials on BC particles. This is consistent with the previous studies showing that the concentration of organics is much larger than those of sulfate and nitrate during the early stage of haze development in Beijing (Guo et al., 2014). The low observed sulfate concentration in this study suggests that the gas phase formation of sulfuric acid was unimportant under our experimental conditions. On the other hand, it has been shown that the aqueous-phase reactions represent the dominate pathway for sulfate formation in Beijing (Guo et al., 2010; Wang et al., 2016).

NO_2 has a higher reaction coefficient with the OH radical (8×10^{-12} cm^3 molecule^{-1} s^{-1}) than SO_2 (Zhang et al., 2015). Nitrate acid formed in the gas phase is transformed into nitrate salts by the reaction with ammonia in the equilibrium process:

$$HNO_3(g) + NH_3(g) \leftrightarrow NH_4NO_3(s) \qquad (8)$$

The equilibrium of this reaction is highly depended on ambient temperature and RH (Zheng et al., 2008). In this study, chamber experiments were conducted in the afternoon with high temperature and low RH (Table 1), which shifted the thermodynamic equilibrium to the gas phase.

4.3 Hygroscopicity evolution

<u>HTDMA measurement</u>

The hygroscopic growth factors (HGF) of particles in each experiment were continuously measured by the HTDMA system and corrected for the reference “dry” diameters,

$$HGF = \frac{D_{wet,t}/D_{m,t}}{D_{dry,0}/D_{m,0}} \qquad (9)$$

where D_m is the mobility diameter of fresh or coated particles at dry condition, D_{dry} is the mobility diameter of particles after experiencing a low humidity (below 30%) cycle in HTDMA, and D_{wet} is the mobility diameter of particles after experiencing a high humidity cycle (87%) in HTDMA.

Figure 10 shows the hygroscopicity variation of BC particles with the initial mobility diameter ($D_{m,0}$) of 100 nm and 150 nm. The measured HGF of 0.999 - 1.004 for fresh BC particles suggests high hydrophobicity, consistent with the previous studies (Khalizov et al., 2009;Weingartner et al., 1997). After exposed to sunlight and ambient gaseous pollutants for several hours, the HGF of these BC particles increased to 1.02-1.08 at the end of each experiment. The HGF value varied with the total growth (ΔD_{me}) of BC particles, but was constant at the same ΔD_{me} for different experiments (Fig. 10). The final HGF values shown in

Figure 10 (1.02-1.08) were much lower than those in previous laboratory studies (Khalizov et al., 2009;Tritscher et al., 2011) but similar to the low hygroscopic fraction in field observations (Swietlicki et al., 2008), even for growth of particle size up to 90 nm in our experiments.

The HGF is affected by many factors, e.g., the particle chemical composition and morphology as well as RH (Qiu et al., 2012). The hygroscopicity of BC particles coated with inorganic components, i.e., sulfuric acid (Khalizov et al., 2009), is significantly higher than that coated by organic compounds (Tritscher et al., 2011). In this study, the major component of the coating substance was LO-OOA with a O/C ratio about 0.5. The low oxygen content of SOA coated on BC particles explains the low hygroscopicity (Jimenez et al., 2009), indicating that coating of BC particles during the early stage haze development in Beijing does not considerably increase the particle hygroscopicity.

The morphology of BC particles directly affects the HGF. As illustrated in Figure 11, when the ΔD_{me} was 18 nm and 22 nm for 100 nm and 150 nm BC particles, respectively, the HGF decreased slightly to about 0.99, suggesting that a thin layer of coatings on BC particles decreased the particle diameter, even though a certain amount of water absorbed by BC particles increased the particle mass. The surface tension of the water layer produced an inward force on the "chain-like" branches of BC particles, leading to particle reconstruction, and a more compact morphology. Such change was also identified in laboratory studies (Weingartner et al., 1997; Tritscher et al., 2011; Qiu et al., 2012). In this study, the BC particles became spherical when ΔD_{me} was 30 nm and 40 nm for particles with initial D_m of 100 nm and 150 nm, respectively (Peng et al., 2016). Therefore, when ΔD_{me} was large, the HGF value was not influenced by reconstruction.

CCN measurements and κ ***closure***

The CCN activation faction (f_{CCN}) of BC particles at different supersaturation during two typical experiments is illustrated in Figure 11. Fresh BC particles were not activated even at very high supersaturation conditions (0.7%). With aging, f_{CCN} rapidly raised to nearly 100% at high supersaturation (0.7% for experiment #4 and 0.6% for experiment #6). After several hours, BC particles became CCN at lower supersaturation. The f_{CCN} at 0.4 supersaturation (Fig. 11a in experiment #4) and 0.3 supersaturation (Fig. 11b in experiment #6) exceeded 50% before the end of these two experiments, suggesting that aging increases the ability of BC particles to become CCN (Wittbom et al., 2014) and a large amount of coatings results in activation at lower supersaturation.

To further investigate the hygroscopicity of BC particles and combine the measurements using HTDMA and CCN, we evaluated the hygroscopicity parameter, kappa (κ) (Petters and Kreidenweis, 2007). The approximate relationship between the dry particle mass equivalent diameter (D_{me}), the critical saturation ratio (Sc) and the apparent κ value of particles is describe as:

$$\kappa = \frac{4A^3}{27D_{me}\ln^2 S_c} \qquad (10)$$

where A is a parameter that includes several features of the solvent,

$$A = \frac{4\sigma_{s/a}M_w}{RT\rho_w} \qquad (11)$$

M_w is the molecular weight of water, ρ_w is the density of water, $\sigma_{s/a}$ is the surface tension of the solution/air interface, R is the universal gas constant, and T is temperature.

In addition to the supersaturated condition, the κ theory also adopts the form for the subsaturated condition, using the HGF from HTDMA measurement and RH:

$$\frac{RH}{exp\left(\frac{A}{D_{wet}}\right)} = \frac{HGF^3 - 1}{HGF^3 - (1-\kappa)} \qquad (12)$$

where D_{wet} is the wet diameter of particles.

The apparent κ values of BC particles calculated by HTDMA (κ_HTDMA) and CCN (κ_CCN) are shown in Figure 11. The κ of fresh BC particles was near zero. With aging, SOA coated on BC particles increased the κ_ HTDMA and κ_ CCN to approximately 0.04, although the κ_ HTDMA and κ_ CCN exhibited difference features. A slightly higher κ_CCN than κ_HTDMA at the beginning of aging was identified, attributed to reconstruction of BC particles after humidified and underestimation of HGF and thus the κ_HTDMA value. Such a difference between κ_CCN and κ_HTDMA was also observed in previous studies (Tritscher et al., 2011; Martin et al., 2013). Nevertheless, the apparent κ values from two both methods were comparable at the end of both experiments.

Assuming that a simple mixing rule is applicable to coated BC particles, the κ for coating materials can be calculated based on the volume fraction of BC and SOA:

$$\kappa = \sum_i \varepsilon_i \kappa_i \qquad (13)$$

where ε_i represents the volume fraction of species *i*. Since the SOA formed inside the chamber was not highly hygroscopic, some of the SOA components might not be able to solve in water droplets (Petters and Kreidenweis, 2008), leading to the underestimation of the κ values of the coating materials in this study.

The κ values of the coating materials were 0.04 at the end of our experiments for both CCN and HTDMA method, much lower than that of ambient aerosols in Beijing (Gunthe et al., 2011; Wu et al., 2016) and those of SOA in previous chamber studies (Jimenez et al., 2009; Tritscher et al., 2011; Martin et al., 2013). As discussed above, the coating substances on BC particles were mainly SOA formed from photochemical oxidation. The κ of SOA depends on the oxidation degree, which is correlated to the O/C ratio (Jimenez et al., 2009; Massoli et al. 2010). The O/C ratio of the coating SOA was 0.5 in our experiment, corresponding to the O/C ratio of approximately 0.4 in Jimenez et al. (2009) and Massoli et al. (2010) duo the utilize of updated AMS calibration method in this study. The κ value of coating materials here is in general slightly lower than those of SOA with similar oxidation degree (O/C ratio) formed from different VOCs precursors (Jimenez et al., 2009; Massoli et al. 2010). As motion above, the κ values of the coating materials might be underestimated duo to the ignore of solubility of the SOA products. Also, our experiments represent the aging of BC under typical urban condition, where variety of anthropogenic VOCs, i.e., toluene, xylene, TMB and small molecular PAHs, contribute significantly to the SOA formation. Some products of these VOC precursors may exhibit low hygroscopicity.

5 Conclusions

In this paper, we present measurements of aging and hygroscopicity of BC particles in Beijing using the QUALITY chamber. The unique two sub-chamber design facilitates the evaluation of aging of BC particles under ambient conditions, by mimicking the ambient gaseous concentrations without the presence of ambient aerosols. High UV transmission efficiency (50-60%) and negligible wall loss of primary gaseous pollutants are shown for the chamber performance. The validation experiments demonstrate little differences in the primary gas concentrations, temperature, and RH between the chamber and the atmosphere, suggesting that the chamber captures the evolution of ambient conditions. In addition, our results show sulfuric acid production correlated with SO_2, indicating that the chamber well simulates photochemical-driven formation of low volatile gaseous species by the hydroxyl radical.

BC aging experiments were performed using the QUALITY chamber in Beijing. Fast growth of BC particles (on average 26±11 nm h^{-1}) was observed, and SOA was identified as the dominate component of the coating materials on BC particles, while inorganic species, such as sulfate and nitrate, were unimportant under our experimental condition and timescale.

The HGF of BC particles exhibited a very low value (1.02-1.08) after several hours aging. A slight decrease of HGF with a thin coating layer indicated reconstruction of BC particles after humidified. Also, a very low kappa value (0.035) for BC particles at both subsaturation and supersaturation conditions were found, with HTDMA and CCN measurements. Hence, our results indicate that initial photochemical aging of BC particles does not appreciably alter the particle hygroscopicity in Beijing.

Acknowledgement

This work was supported by National Natural Science Foundation of China (91544214, 41421064), the National Basic Research Program, China Ministry of Science and Technology (Grant 2013CB228503, Grant 2013CB955801), National Natural Science Foundation of China (Grant 21190052), and the China Ministry of Environmental Protection's Special Funds for Scientific Research on Public Welfare (Grant 20130916). R.Z. acknowledged support from the Robert A. Welch Foundation (Grant A-1417) and Houston Advanced Research Center. We thanked Wei Hu and Zhaoheng Gong for their assistance with the AMS data analysis, Wentai Chen and Yue Li for providing VOCs data.

References

Bond, T. C., Doherty, S. J., Fahey, D. W., Forster, P. M., Berntsen, T., DeAngelo, B. J., Flanner, M. G., Ghan, S., Kärcher, B., Koch, D., Kinne, S., Kondo, Y., Quinn, P. K., Sarofim, M. C., Schultz, M. G., Schulz, M., Venkataraman, C., Zhang, H., Zhang, S., Bellouin, N., Guttikunda, S. K., Hopke, P. K., Jacobson, M. Z., Kaiser, J. W., Klimont, Z., Lohmann, U., Schwarz, J. P., Shindell, D., Storelvmo, T., Warren, S. G., and Zender, C. S.: Bounding the role of black carbon in the climate system: A scientific assessment, Journal of Geophysical Research: Atmospheres, 118, 5380-5552, 10.1002/jgrd.50171, 2013.

Canagaratna, M. R., Jimenez, J. L., Kroll, J. H., Chen, Q., Kessler, S. H., Massoli, P., Hildebrandt Ruiz, L., Fortner, E., Williams, L. R., Wilson, K. R., Surratt, J. D., Donahue, N. M., Jayne, J. T., and Worsnop, D. R.: Elemental ratio measurements of organic compounds using aerosol mass spectrometry: characterization, improved calibration, and implications, Atmos. Chem. Phys., 15, 253-272, doi:10.5194/acp-15-253-2015, 2015.

Claeys, M.: Formation of Secondary Organic Aerosols Through Photooxidation of Isoprene, Science, 303, 1173-1176, doi:10.1126/science.1092805, 2004.

DeCarlo, P. F., Slowik, J. G., Worsnop, D. R., Davidovits, P., and Jimenez, J. L.: Particle Morphology and Density Characterization by Combined Mobility and Aerodynamic Diameter Measurements. Part 1: Theory, Aerosol Sci. Tech., 38, 1185-1205, 10.1080/027868290903907, 2004.

DeCarlo, P. F., Kimmel, J. R., Trimborn, A., Northway, M. J., Jayne, J. T., Aiken, A. C., Gonin, M., Fuhrer, K., Horvath, T., Docherty, K. S., Worsnop, D. R., and Jimenez, J. L.: Field-deployable, high-resolution, time-of-flight aerosol mass spectrometer, Anal. Chem., 78, 8281-8289, doi:10.1021/ac061249n, 2006.

DeCarlo, P. F., Ulbrich, I. M., Crounse, J., de Foy, B., Dunlea, E. J., Aiken, A. C., Knapp, D., Weinheimer, A. J., Campos, T., Wennberg, P. O., and Jimenez, J. L.: Investigation of the sources and processing of organic aerosol over the Central Mexican Plateau from aircraft measurements during MILAGRO, Atmos. Chem. Phys., 10, 5257-5280, doi:10.5194/acp-10-5257-2010, 2010.

Ervens, B., Turpin, B. J., and Weber, R. J.: Secondary organic aerosol formation in cloud droplets and aqueous particles (aqSOA): a review of laboratory, field and model studies, Atmos. Chem. Phys., 11, 11069-11102, doi:10.5194/acp-11-11069-2011, 2011.

Fortner, E. C., Zhao, J., and Zhang, R. Y.: Development of ion drift-chemical ionization mass spectrometry, Anal. Chem., 76, 5436-5440, doi:10.1021/ac0493222, 2004.

Gunthe, S. S., Rose, D., Su, H., Garland, R. M., Achtert, P., Nowak, A., Wiedensohler, A., Kuwata, M., Takegawa, N., Kondo, Y., Hu, M., Shao, M., Zhu, T., Andreae, M. O., and Pöschl, U.: Cloud condensation nuclei (CCN) from fresh and aged air pollution in the megacity region of Beijing, Atmos. Chem. Phys., 11, 11023-11039, doi:10.5194/acp-11-11023-2011, 2011.

Guo, S., Hu, M., Lin, Y., Gomez-Hernandez, M., Zamora, M. L., Peng, J. F., Collins, D. R., and Zhang, R. Y.: OH-Initiated Oxidation of m-Xylene on Black Carbon Aging, Environ. Sci. Technol., 50, 8605-8612, doi:10.1021/acs.est.6b01272, 2016.

Guo, S., Hu, M., Wang, Z. B., Slanina, J., and Zhao, Y. L.: Size-resolved aerosol water-soluble ionic compositions in the summer of Beijing: implication of regional secondary formation, Atmos. Chem. Phys., 10, 947-959, 2010.

Guo, S., Hu, M., Zamora, M. L., Peng, J., Shang, D., Zheng, J., Du, Z., Wu, Z., Shao, M., Zeng, L., Molina, M. J., and Zhang, R.: Elucidating severe urban haze formation in China, P. Natl. Acad. Sci. USA, 111, 17373-17378, doi:10.1073/pnas.1419604111, 2014.

He, L.-Y., X.-F. Huang, L. Xue, M. Hu, Y. Lin, J. Zheng, R. Zhang, and Y.-H. Zhang: Submicron aerosol analysis and organic source apportionment in an urban atmosphere in Pearl River Delta of China using high-resolution aerosol mass spectrometry, J. Geophys. Res. 116, D12304, doi:10.1029/2010JD014566, 2011.

Hu, M., Peng, J., Sun, K., Yue, D., Guo, S., Wiedensohler, A., and Wu, Z.: Estimation of Size-Resolved Ambient Particle Density Based on the Measurement of Aerosol Number, Mass, and Chemical Size Distributions in the Winter in Beijing, Environ. Sci. Technol., 46, 9941-9947, doi:10.1021/es204073t, 2012.

Hu, W., Hu, M., Hu, W., Jimenez, J. L., Yuan, B., Chen, W., Wang, M., Wu, Y., Chen, C., Wang, Z., Peng, J., Zeng, L., and Shao, M.: Chemical composition, sources and aging process of sub-micron aerosols in Beijing: contrast between summer and winter, J. Geophys. Res.- Atmos., 121, 1955-1977 doi:10.1002/2015jd024020, 2016.

Huang, X. F., He, L. Y., Hu, M., Canagaratna, M. R., Sun, Y., Zhang, Q., Zhu, T., Xue, L., Zeng, L. W., Liu, X. G., Zhang, Y. H., Jayne, J. T., Ng, N. L., and Worsnop, D. R.: Highly time-resolved chemical characterization of atmospheric submicron particles during 2008 Beijing Olympic Games using an Aerodyne High-Resolution Aerosol Mass Spectrometer, Atmos. Chem. Phys., 10, 8933-8945, doi:10.5194/acp-10-8933-2010, 2010.

Intergovernmental Panel on Climate Change (IPCC), Climate Change 2013: The Physical Science Basis, Cambridge Univ. Press, Cambridge, UK, 2013.

Jacobson, M. Z.: Strong radiative heating due to the mixing state of black carbon in atmospheric aerosols, Nature, 409, 695-697, doi:10.1038/35055518, 2001.

Jimenez, J. L., Canagaratna, M. R., Donahue, N. M., Prevot, A. S. H., Zhang, Q., Kroll, J. H., DeCarlo, P. F., Allan, J. D., Coe, H., Ng, N. L., Aiken, A. C., Docherty, K. S., Ulbrich, I. M., Grieshop, A. P., Robinson, A. L., Duplissy, J., Smith, J. D., Wilson, K. R., Lanz, V. A., Hueglin, C., Sun, Y. L., Tian, J., Laaksonen, A., Raatikainen, T., Rautiainen, J., Vaattovaara, P., Ehn, M., Kulmala, M., Tomlinson, J. M., Collins, D. R., Cubison, M. J., Dunlea, J., Huffman, J. A., Onasch, T. B., Alfarra, M. R., Williams, P. I., Bower, K., Kondo, Y., Schneider, J., Drewnick, F., Borrmann, S., Weimer, S., Demerjian, K., Salcedo, D., Cottrell, L., Griffin, R., Takami, A., Miyoshi, T., Hatakeyama, S., Shimono, A., Sun, J. Y., Zhang, Y. M., Dzepina, K., Kimmel, J. R., Sueper, D., Jayne, J. T., Herndon, S. C., Trimborn, A. M., Williams, L. R., Wood, E. C., Middlebrook, A. M., Kolb, C. E., Baltensperger, U., and Worsnop, D. R.: Evolution of Organic Aerosols in the Atmosphere, Science, 326, 1525-1529, doi:10.1126/science.1180353, 2009.

Kalberer, M.: Identification of Polymers as Major Components of Atmospheric Organic Aerosols, Science, 303, 1659-1662, doi:10.1126/science.1092185, 2004.

Khalizov, A. F., Xue, H., and Zhang, R.: Enhanced light absorption and scattering by carbon soot aerosols internally mixed with sulfuric acid, J. Phys. Chem., 113, 1066–1074, doi:10.1021/jp807531n, 2009.

Khalizov, A. F., Zhang, R., Zhang, D., Xue, H., Pagels, J., and McMurry, P. H.: Formation of highly hygroscopic soot aerosols upon internal mixing with sulfuric acid vapor, J. Geophys. Res., 114, doi:10.1029/2008jd010595, 2009.

Khalizov, A. F., Lin, Y., Qiu, C., Guo, S., Collins, D., and Zhang, R.: Role of OH-Initiated Oxidation of Isoprene in Aging of Combustion Soot, Environ. Sci. Technol., 47, 2254-2263, doi:10.1021/es3045339, 2013.

Kuwata, M., Kondo, Y., Mochida, M., Takegawa, N., and Kawamura, K.: Dependence of CCN activity of less volatile particles on the amount of coating observed in Tokyo, J. Geophys. Res., 112, doi:10.1029/2006jd007758, 2007.

Liu, S., Aiken, A. C., Gorkowski, K., Dubey, M. K., Cappa, C. D., Williams, L. R., Herndon, S. C., Massoli, P., Fortner, E. C., Chhabra, P. S., Brooks, W. A., Onasch, T. B., Jayne, J. T., Worsnop, D. R., China, S., Sharma, N., Mazzoleni, C., Xu, L., Ng, N. L., Liu, D., Allan, J. D., Lee, J. D., Fleming, Z. L., Mohr, C., Zotter, P., Szidat, S., and Prevot, A. S. H.: Enhanced light absorption by mixed source black and brown carbon particles in UK winter, Nat. Commun., 6, Artn 8435, doi:10.1038/Ncomms9435, 2015.

Liu, Y., Shao, M., Fu, L. L., Lu, S. H., Zeng, L. M., and Tang, D. G.: Source profiles of volatile organic compounds (VOCs) measured in China: Part I, Atmospheric Environment, 42, 6247-6260, doi:10.1016/j.atmosenv.2008.01.070, 2008.

Ma, Y., Brooks, S. D., Vidaurre, G., Khalizov, A. F., Wang, L., and Zhang, R.: Rapid modification of cloud-nucleating ability of aerosols by biogenic emissions, Geophys. Res. Lett., 40, 6293-6297, doi:10.1002/2013gl057895, 2013.

Martin, M., Tritscher, T., Jurányi, Z., Heringa, M. F., Sierau, B., Weingartner, E., Chirico, R., Gysel, M., Prévôt, A. S. H., Baltensperger, U., and Lohmann, U.: Hygroscopic properties of fresh and aged wood burning particles, J. Aerosol Sci., 56, 15-29, doi:10.1016/j.jaerosci.2012.08.006, 2013.

Massoli, P., Lambe, A. T., Ahern, A. T., Williams, L. R., Ehn, M., Mikkilä, J., Canagaratna, M. R., Brune, W. H., Onasch, T. B., Jayne, J. T., Petäjä, T., Kulmala, M., Laaksonen, A., Kolb, C. E., Davidovits, P., Worsnop, D. R.: Relationship between aerosol oxidation level and hygroscopic properties of laboratory generated secondary organic aerosol (SOA) particles. Geophys. Res. Lett., 37, L24801, doi:10.1029/2010GL045258, 2010.Moffet, R. C., and Prather, K. A.: In-situ measurements of the mixing state and optical properties of soot with implications for radiative forcing estimates, P. Natl. Acad. Sci. USA, 106, 11872-11877, doi:10.1073/pnas.0900040106, 2009.

Pagels, J., McMurry, P.H., Khalizov, A.F., and Zhang, R.: Processing of soot by controlled sulphuric acid and water condensation—Mass and mobility relationship, Aerosol Sci. Tech. 43, 629–640, 2009.

Peng, J., Hu, M., Du, Z., Wang, Y., Zheng, J., Zhang, W., Yang, Y., Qin, Y., Zheng, R., Xiao, Y., Wu, Y., Lu, S., Wu, Z., Guo, S., Mao, H., and Shuai, S.: Gasoline aromatic: a critical determinant of urban secondary organic aerosol formation, Atmos. Chem. Phys. Discuss., doi:10.5194/acp-2017-254, 2017.

Peng, J. F., Hu, M., Guo, S., Du, Z. F., Zheng, J., Shang, D. J., Zamora, M. L., Zeng, L. M., Shao, M., Wu, Y. S., Zheng, J., Wang, Y., Glen, C. R., Collins, D. R., Molina, M. J., and Zhang, R. Y.: Markedly enhanced absorption and direct radiative forcing of black carbon under polluted urban environments, P. Natl. Acad. Sci. USA, 113, 4266-4271, doi:10.1073/pnas.1602310113, 2016.

Peng, J. F., Hu, M., Wang, Z. B., Huang, X. F., Kumar, P., Wu, Z. J., Guo, S., Yue, D. L., Shang, D. J., Zheng, Z., and He, L. Y.: Submicron aerosols at thirteen diversified sites in

China: size distribution, new particle formation and corresponding contribution to cloud condensation nuclei production, Atmos. Chem. Phys., 14, 10249-10265, doi:10.5194/acp-14-10249-2014, 2014.

Petters, M. D., and Kreidenweis, S. M.: A single parameter representation of hygroscopic growth and cloud condensation nucleus activity, Atmos. Chem. Phys., 7, 1961-1971, 2007.

Petters, M. D., and Kreidenweis, S. M.: A single parameter representation of hygroscopic growth and cloud condensation nucleus activity—Part 2: Including solubility, Atmos. Chem. Phys., 8, 6273– 6279, 2008.

Qiu, C., Khalizov, A. F., and Zhang, R. Y.: Soot Aging from OH-Initiated Oxidation of Toluene, Environ. Sci. Technol., 46, 9464-9472, doi:10.1021/Es301883y, 2012.

Qiu, C., and Zhang, R.: Multiphase chemistry of atmospheric amines, Phys. Chem. Chem. Phys. 15, doi:10.1039/C3CP43446J, 5738-5752, 2013.

Reed, R. C.: Observations of secondary organic aerosol production and soot aging under atmospheric conditions using a novel new environmental aerosol chamber, PhD dissertation, Texas A&M Univ, College Station, TX,. 2010.

Ruehl, C. R., Davies, J. F., and Wilson, K. R.: An interfacial mechanism for cloud droplet formation on organic aerosols, Science, 351, 1447-1450, doi:10.1126/science.aad4889, 2016.

Saathoff, H., Naumann, K. H., Schnaiter, M., Schöck, W., Möhler, O., Schurath, U., Weingartner, E., Gysel, M., and Baltensperger, U.: Coating of soot and (NH4)2SO4 particles by ozonolysis products of α-pinene, J. Aerosol Sci., 34, 1297-1321, doi:10.1016/s0021-8502(03)00364-1, 2003.

Santoro, R. J., Semerjian, H. G., and Dobbins, R. A.: Soot Particle Measurements in Diffusion Flames, Combust. Flame, 51, 203-218, 1983.

Swietlicki, E., Hansson, H. C., HÄMeri, K., Svenningsson, B., Massling, A., McFiggans, G., McMurry, P. H., PetÄJÄ, T., Tunved, P., Gysel, M., Topping, D., Weingartner, E., Baltensperger, U., Rissler, J., Wiedensohler, A., and Kulmala, M.: Hygroscopic properties of submicrometer atmospheric aerosol particles measured with H-TDMA instruments in various environments—a review, Tellus B, 60, 432-469, doi:10.1111/j.1600-0889.2008.00350.x, 2008.

Tritscher, T., Jurányi, Z., Martin, M., Chirico, R., Gysel, M., Heringa, M. F., DeCarlo, P. F., Sierau, B., Prévôt, A. S. H., Weingartner, E., and Baltensperger, U.: Changes of hygroscopicity and morphology during ageing of diesel soot, Environ. Res. Lett., 6, 034026, doi:10.1088/1748-9326/6/3/034026, 2011.

Wang, G. H., Zhang, R. Y., Gomez, M. E., Yang, L. X., Zamora, M. L., Hu, M., Lin, Y., Peng, J. F., Guo, S., Meng, J. J., Li, J. J., Cheng, C. L., Hu, T. F., Ren, Y. Q., Wang, Y. S., Gao, J., Cao, J. J., An, Z. S., Zhou, W. J., Li, G. H., Wang, J. Y., Tian, P. F., Marrero-Ortiz, W., Secrest, J., Du, Z. F., Zheng, J., Shang, D. J., Zeng, L. M., Shao, M., Wang, W. G., Huang, Y., Wang, Y., Zhu, Y. J., Li, Y. X., Hu, J. X., Pan, B., Cai, L., Cheng, Y. T., Ji, Y. M., Zhang, F., Rosenfeld, D., Liss, P. S., Duce, R. A., Kolb, C. E., and Molina, M. J.: Persistent sulfate formation from London Fog to Chinese haze, P. Natl. Acad. Sci. USA, 113, 13630-13635, doi:10.1073/pnas.1616540113, 2016.

Wang, L., Khalizov, A. F., Zheng, J., Xu, W., Ma, Y., Lal, V., and Zhang, R. Y.: Atmospheric nanoparticles formed from heterogeneous reactions of organics, Nat. Geosci., 3, 238-242, doi:10.1038/NGEO778, 2010.

Wang, Y., Wan, Q., Meng, W., Liao, F., Tan, H., and Zhang, R.: Long-term impacts of aerosols on precipitation and lightning over the Pearl River Delta megacity area in China, Atmos. Chem. Phys. 11, 12421–12436, 2011.

Wang, Y., Khalizov, A., Levy, M., and Zhang, R.: Light absorbing aerosols and their atmospheric impacts, Atmos. Environ. 81, 713-715, doi:10.1016/j.atmosenv.2013.09.034, 2013.

Weingartner, E., Burtscher, H., and Baltensperger, U.: Hygroscopic properties of carbon and diesel soot particles, Atmos. Environ., 31, 2311-2327, doi:10.1016/S1352-2310(97)00023-X, 1997.

Wittbom, C., Eriksson, A. C., Rissler, J., Carlsson, J. E., Roldin, P., Nordin, E. Z., Nilsson, P. T., Swietlicki, E., Pagels, J. H., and Svenningsson, B.: Cloud droplet activity changes of soot aerosol upon smog chamber ageing, Atmos. Chem. Phys., 14, 9831-9854, doi:10.5194/acp-14-9831-2014, 2014.

Wu, Z. J., Zheng, J., Shang, D. J., Du, Z. F., Wu, Y. S., Zeng, L. M., Wiedensohler, A., and Hu, M.: Particle hygroscopicity and its link to chemical composition in the urban atmosphere of Beijing, China, during summertime, Atmos. Chem. Phys., 16, 1123-1138, doi:10.5194/acp-16-1123-2016, 2016.

Xue, H., Khalizov, A. F., Wang, L., Zheng, J., and Zhang, R.: Effects of dicarboxylic acid coating on the optical properties of soot, Phys. Chem. Chem. Phys., 11, 7865-7875, doi:10.1039/b700001a, 2009a.

Xue, H., Khalizov. A F., and Zhang, R.: Effects of coating of dicarboxylic acids on the mass-mobility relationship of soot particles, Environ. Sci. Technol. 43, 2787–2792, doi: 10.1021/es803287v, 2009b.

Yuan, T., Li, Z., Zhang, R., and Fan, J.: Increase of cloud droplet size with aerosol optical depth: An observation and modeling study, J. Geophys. Res., 113, D04201, doi:10.1029/2007JD008632, 2008.

Zhang, D., and Zhang R.: Laboratory investigation of heterogeneous interaction of sulfuric acid with soot, Environ. Sci. Technol. 39, 5722-5727, doi:10.1021/es050372d, 2005.

Zhang, R., Khalizov, A. F., Pagels, J., Zhang, D., Xue, H., and McMurry, P. H.: Variability in morphology, hygroscopicity, and optical properties of soot aerosols during atmospheric processing, P. Natl. Acad. Sci. USA, 105, 10291-10296, doi:10.1073/pnas.0804860105, 2008.

Zhang, R. Y., Suh, I., Zhao, J., Zhang, D., Fortner, E. C., Tie, X. X., Molina, L. T., and Molina, M. J.: Atmospheric new particle formation enhanced by organic acids, Science, 304, 1487-1490, doi:10.1126/science.1095139, 2004.

Zhang, R., Khalizov, A.F., Wang, L., Hu, M., Xu, W.: Nucleation and growth of nanoparticles in the atmosphere, Chem. Rev., 112, 1957-2011, doi:10.1021/cr2001756, 2012.

Zhang, R. Y., Wang, G. H., Guo, S., Zarnora, M. L., Ying, Q., Lin, Y., Wang, W. G., Hu, M., and Wang, Y.: Formation of Urban Fine Particulate Matter, Chem. Rev., 115, 3803-3855, doi:10.1021/acs.chemrev.5b00067, 2015.

Zhao, J., Levitt, N. P., Zhang, R., and Chen, J.: Heterogeneous reactions of methylglyoxal in acidic media: Implications for secondary organic aerosol formation, Environ. Sci.

Technol., 40, 7682-7687, doi:10.1021/es060610k, 2006.

Zhao, J., Khalizov, A.F., Zhang, R., and McGraw, R.: Hydrogen bonding interaction of molecular complexes and clusters of aerosol nucleation precursors, J. Phys. Chem., 113, 680–689, doi:10.1021/jp806693r, 2009.

Zhao, P. S., Dong, F., He, D., Zhao, X. J., Zhang, X. L., Zhang, W. Z., Yao, Q., and Liu, H. Y.: Characteristics of concentrations and chemical compositions for PM2.5 in the region of Beijing, Tianjin, and Hebei, China, Atmos. Chem. Phys., 13, 4631-4644, doi:10.5194/acp-13-4631-2013, 2013.

Zheng, J., Zhang, R., Fortner, E. C., Volkamer, R. M., Molina, L., Aiken, A. C., Jimenez, J. L., Gaeggeler, K., Dommen, J., Dusanter, S., Stevens, P.S., and Tie, X.: Measurements of HNO_3 and N_2O_5 using ion drift - chemical ionization mass spectrometry during the MCMA - 2006 campaign, Atmos. Chem. Phys., 8, 6823–6838, 2008.

Zheng, J., Khalizov, A., Wang, L., and Zhang, R. Y.: Atmospheric Pressure-Ion Drift Chemical Ionization Mass Spectrometry for Detection of Trace Gas Species, Anal. Chem., 82, 7302-7308, doi:10.1021/ac101253n, 2010.

Table 1. Summary of ambient conditions for BC aging experiments conducted in Beijing. The $PM_{2.5}$, gas concentrations and meteorological condition were averaged from the entire experimental time. D_m and T represent the mobility diameter and temperature, respectively.

No.	Date	Time		Initial Dm (nm)	$PM_{2.5}$ ($\mu g\ m^{-3}$)	$J(O^1D)$ (10^{-6})	Gas Concentration (ppb)					Meteorological Conditions	
		Start	End				Toluene	Xylene	SO_2	NO_x	O_3	T (°C)	RH (%)
#1	Aug. 18th	12:41	14:47	95	43	19	0.49	0.13	1.7	8.8	56	35	27
#2	Aug. 22nd	13:32	16:51	96	69	3.7	3.41	0.78	2	36.1	26	26	69
#3	Sep. 7th	12:40	14:52	97	12	17.5	0.71	0.17	2.7	10.2	75	30	35
#4	Sep. 9th	13:13	17:06	97	40	6.3	0.77	0.21	4	11	68	26	50
#5	Sep. 1st	13:19	16:13	147	27	11.6	0.76	0.19	4.6	19.9	83	31	33
#6	Sep. 11st	13:50	17:25	147	57	6.1	1.57	0.39	6.7	17.1	92	29	42
#7	Sep. 21st	15:31	17:41	146	30	2.1	0.75	0.29	2	10.6	90	28	37
#8	Aug. 24th	11:37	16:06	216	8.8	21.1	0.98	0.3	1.7	15.6	57	36	25
#9	Sep. 5th	14:06	16:44	220	12	8.3	0.45	0.2	2.2	14.6	54	29	35
#10	Oct. 17th	12:54	17:13	224	57	3.2	-	-	13.8	41	34	18	30

Table 2. Summary of particle properties for BC aging experiments conducted in Beijing. D_m, ρ_{eff} and D_{me} represent the mobility diameter, effective density and mass equivalent diameter, respectively.

		D_m		**ρ_{eff}**		**D_{me}**			
No.	**Date**	**Initial (nm)**	**Final (nm)**	**Initial (g cm^{-3})**	**Final (g cm^{-3})**	**Initial (nm)**	**Final (nm)**	**ΔD_{me} (nm)**	**Growth Rate[a] (nm h^{-1})**
#1	Aug. 18th	95	157	0.50	1.35	62	162	100	47
#2	Aug. 22nd	96	129	0.46	1.31	61	126	65	20
#3	Sep. 7th	97	147	0.45	1.25	62	142	80	36
#4	Sep. 9th	97	136	0.43	1.30	61	133	62	19
#5	Sep. 1st	147	170	0.34	1.36	85	168	83	29
#6	Sep. 11st	147	162	0.34	1.34	84	159	75	20
#7	Sep. 21st	146	132	0.34	1.05	84	116	32	15
#8	Aug. 24th	216	272	0.32	1.37	123	275	152	34
#9	Sep. 5th	220	202	0.25	1.33	114	197	83	31
#10	Oct. 17th	224	224	0.24	0.52	117	157	40	11
Average								**77±33**	**26±11**

[a] The growth rate is calculated using the data between 12:00 and 17:00 for each experiment.

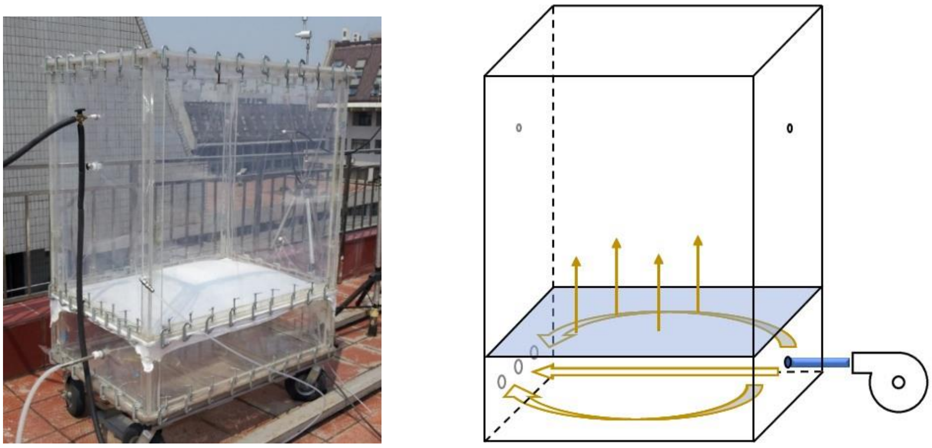

Figure 1. Photo (left) and schematic (right) of the quasi-atmospheric aerosol evolution study (QUALITY) chamber

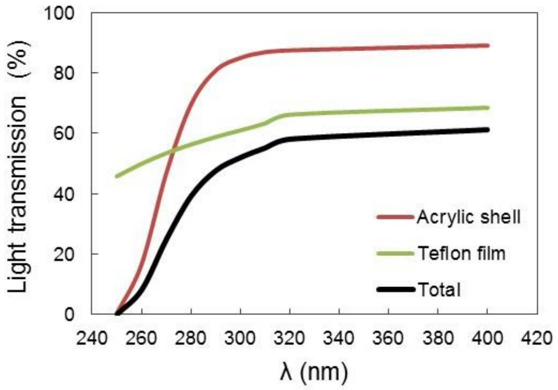

Figure 2. Light transmission spectra of the PFA Teflon film (yellow line), the acrylite shell (red line), and their total transmission in the UV range (black line).

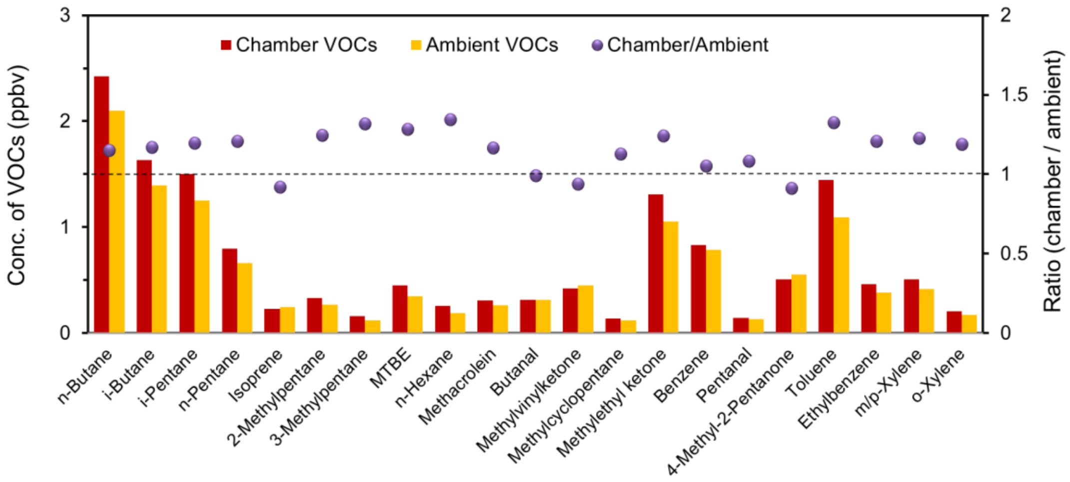

Figure 3. Comparison of VOCs concentrations in the QUALITY chamber (red bar) and in the ambient air (yellow bar) before the start of BC aging experiment. Purple cycles represent the ratio of each species in the reaction chamber to in the ambient air. Only the VOCs species that contains 4 or more carbons with the concentration higher than 0.1 ppb are shown in the figure.

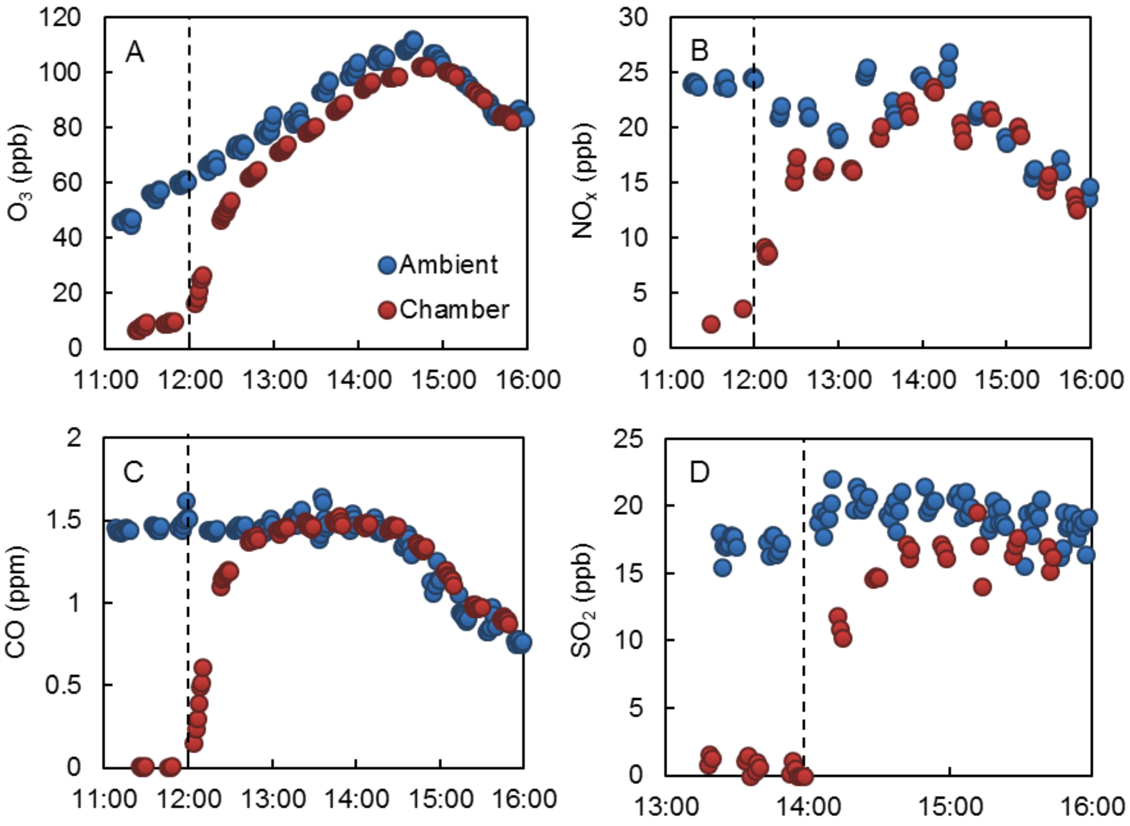

Figure 4. Concentrations of O_3 (A), NO_x (B), CO (C), and SO_2 (D) measured inside the QUALITY chamber (Red circles) and in the ambient air (blue circles). The vertical dashed lines denote the time when the ambient air started to be pulled through the bottom flow chamber and the ambient gases began to exchange into the upper reaction chamber.

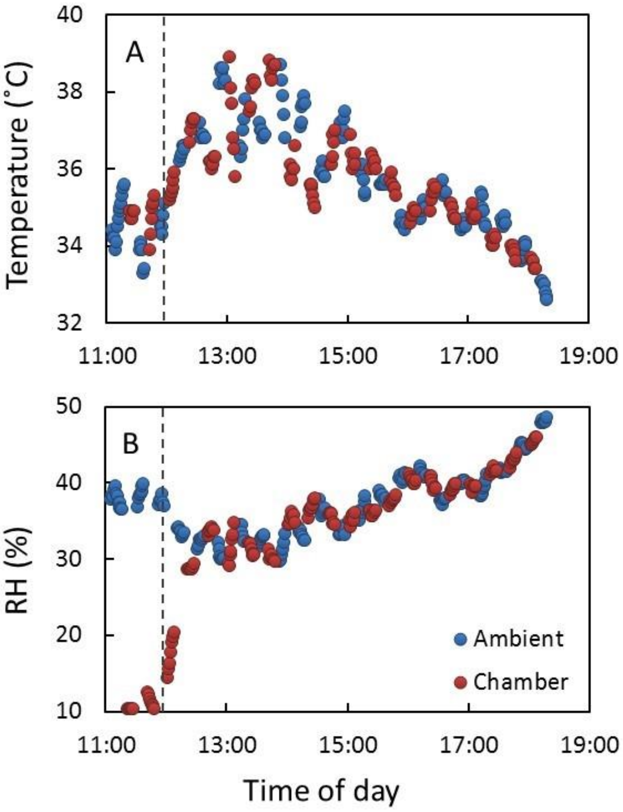

Figure 5. Temperature (A) and RH (B) measured inside the QUALITY chamber (Red circles) and in the ambient air (blue circles). The temperature and RH were measured by probes placed in the sampling tube adjacent to the chamber. The vertical dashed lines denote the time when the ambient air started to be pulled through the bottom flow chamber and the ambient gases began to exchange into the upper reaction chamber.

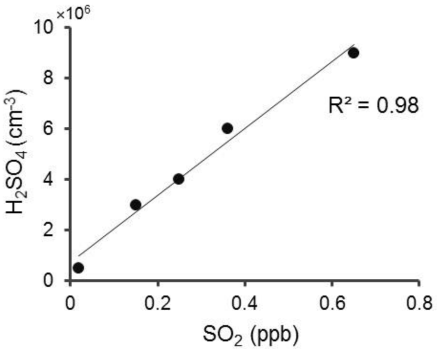

Figure 6. Sulfuric acid concentration as function of SO_2 concentration inside the chamber

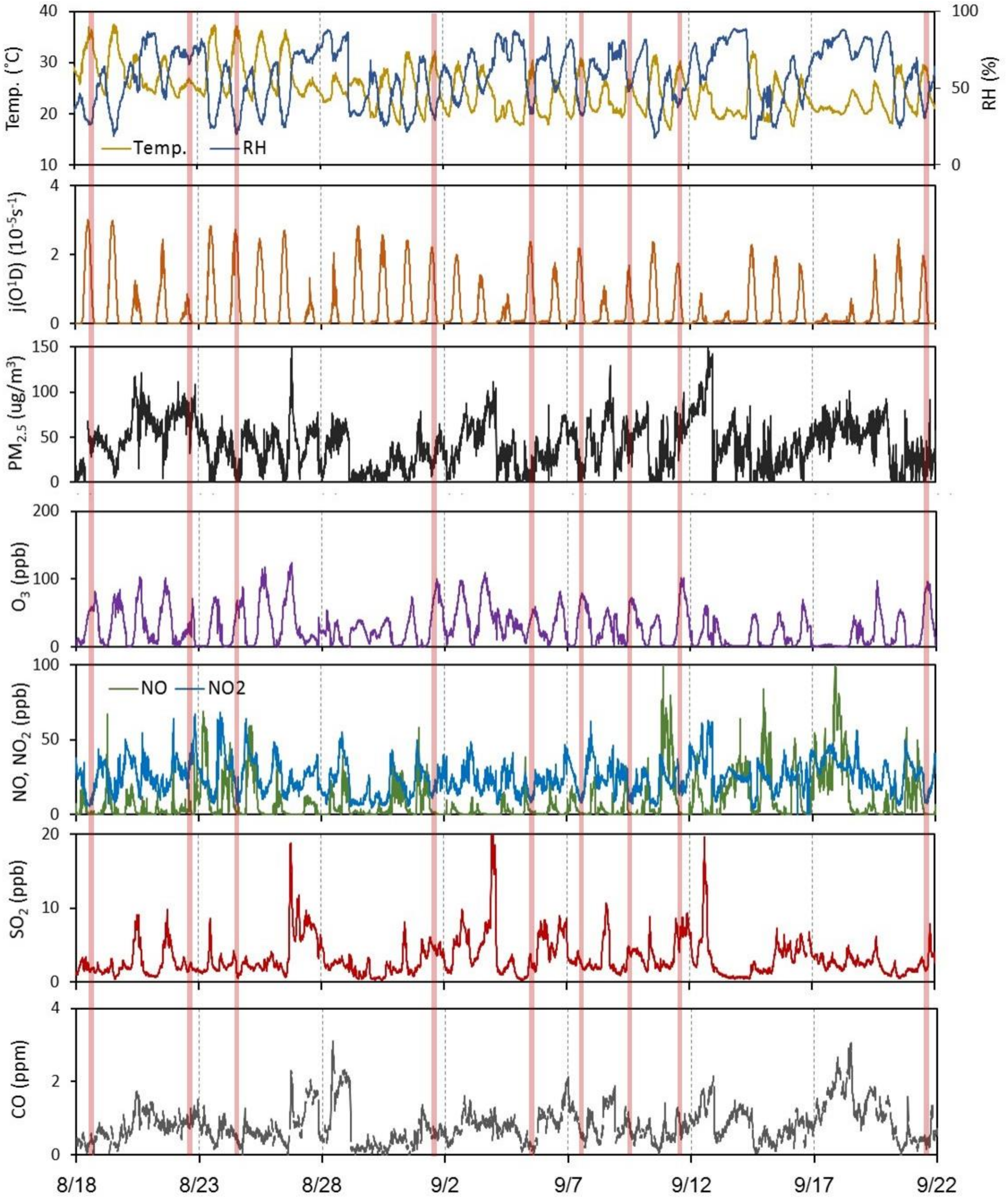

Figure 7. Time series of ambient pollutant concentrations and meteorological parameters during the experimental period in Beijing. Red bars indicate periods when BC aging experiments were conducted.

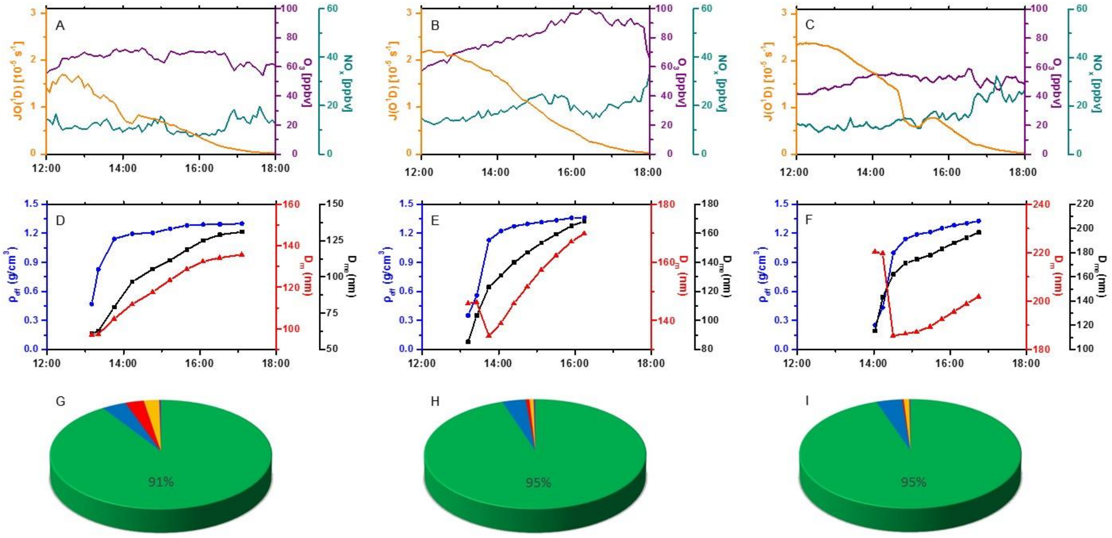

Figure 8. Ambient condition (A, B，C), changes of diameter and density of BC particle (D, E, F), and the chemical composition of coating materials (G, H, I) during three typical aging experiments. A and D correspond to experiment #4; B and E correspond to experiment #5, and C and E correspond to experiment #9. D_m is the peak mobility diameter of BC particles, ρ_{eff} is the best-fit effective density of BC particles with the mobility diameter D_m, D_{me} is the mass equivalent diameter of BC particles, and $J(O^1D)$ represents the measured photolysis rate constant for $O(^1D)$. The colors of green, blue, red, yellow and purple in the pie charts represent organics, nitrate, sulfate, ammonium, and chlorine, respectively. The numbers in figure G, H and I are the mass fraction of organics.

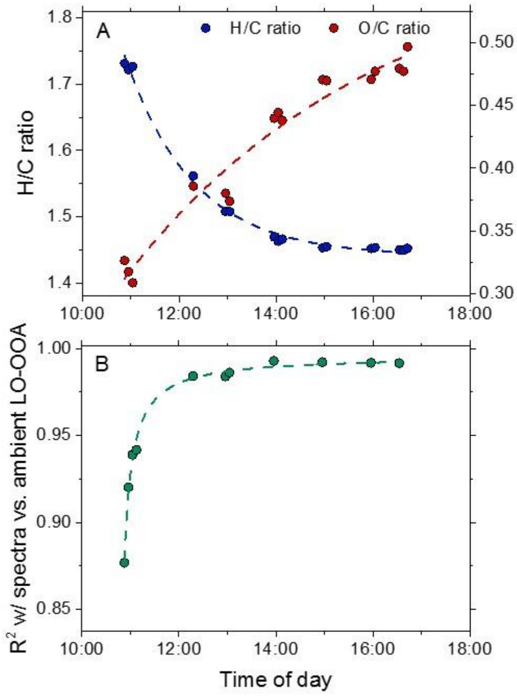

Figure 9. The evolution of organic aerosols inside the chamber during an aging experiment (#8) in Beijing. (A) the H/C and O/C ratios of organics on aged BC particles; (b) the correlation coefficients (R^2) between the evolving total OA spectra in chamber experiment and the LO-OOA spectra derived from the Beijing field data set.

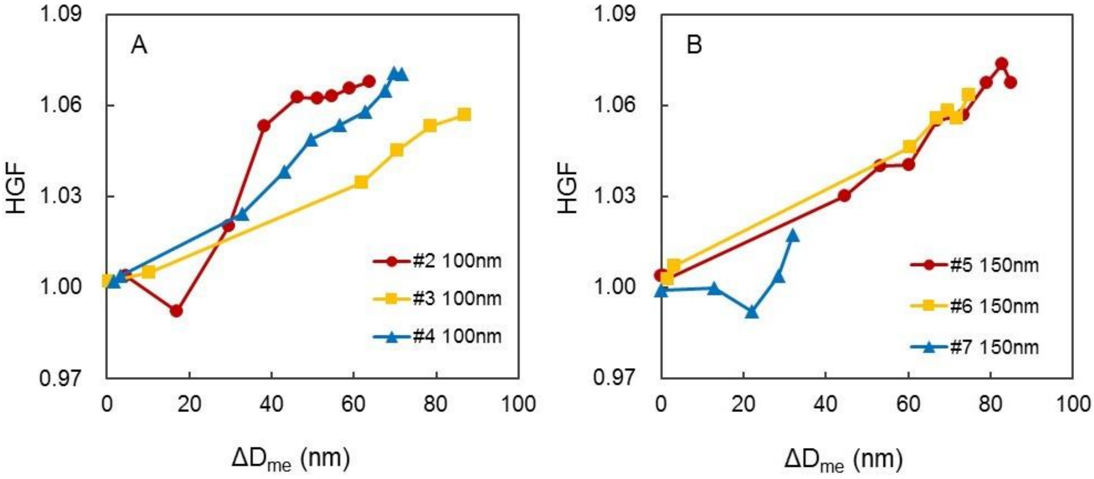

Figure 10. Evolution of hygroscopic growth factors (HGF) of BC particles during aging as a function of ΔD_{me}. (A) three experiments with 100 nm BC particle; (B) three experiments with 150 nm BC particle. Different colors in each figure represent different experiments. Hygroscopicity measurement is not available for experiment #1.

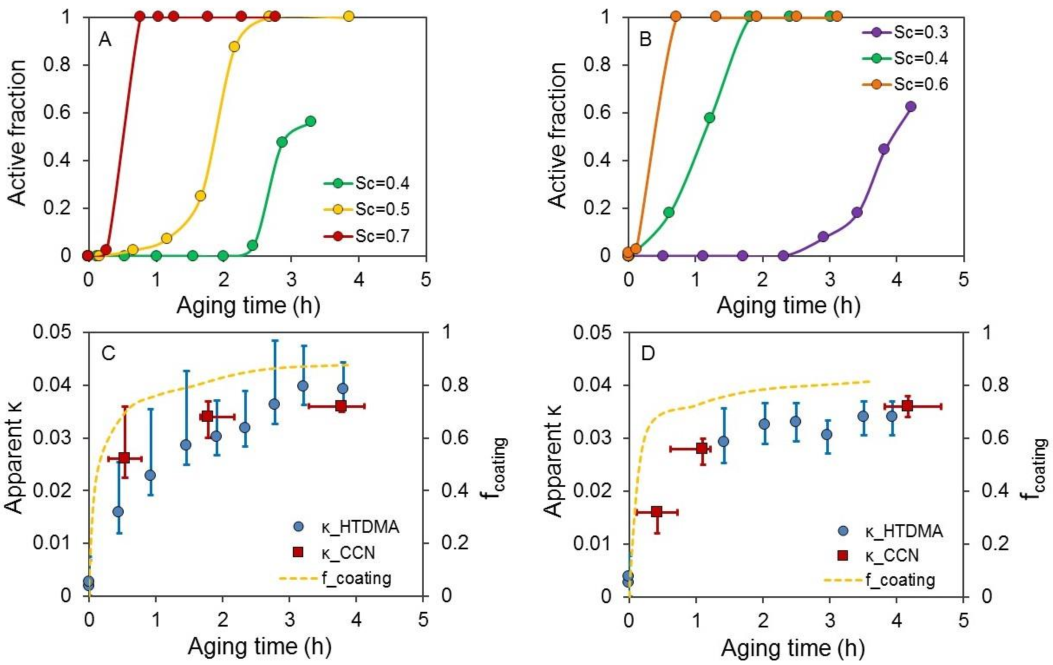

Figure 11. The active fraction of BC particles under diversified supersaturation (A, B) and the closure of apparent κ for BC particles with initial diameter (C, D) during aging in two typical experiments. A, C are the results from experiment #4 with 100nm BC particles and B, D represents experiment #6 with 150nm BC particles. Red squre and blue circle in C and D represent the apparent κ calculated using CCN counter data and HTDMA data, respectively. Yellow slash line represents the fraction of coating materials on BC particles. The error bars of κ_CCN and κ_HTDMA represent the uncertainty in the calculation.